JACS
JOURNAL OF THE AMERICAN CHEMICAL SOCIETY
pubs.acs.org/JACS
Article

A Successive Conversion−Deintercalation Delithiation Mechanism for Practical Composite Lithium Anodes

Peng Shi, Li-Peng Hou, Cheng-Bin Jin, Ye Xiao, Yu-Xing Yao, Jin Xie, Bo-Quan Li, Xue-Qiang Zhang,* and Qiang Zhang*

Cite This: https://doi.org/10.1021/jacs.1c08606
Read Online
ACCESS | Metrics & More | Article Recommendations | Supporting Information

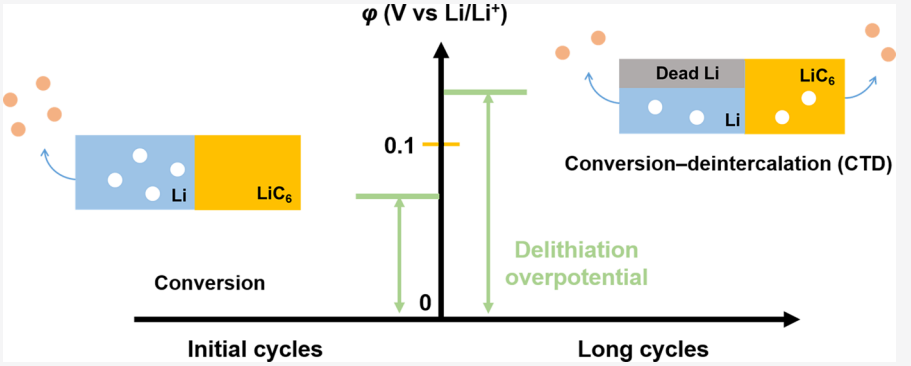

ABSTRACT: Lithium (Li) metal anodes are attractive for high-energy-density batteries. Dead Li is inevitably generated during the delithiation of deposited Li based on a conversion reaction, which severely depletes active Li and electrolyte and induces a short lifespan. In this contribution, a successive conversion−deintercalation (CTD) delithiation mechanism is proposed by manipulating the overpotential of the anode to restrain the generation of dead Li. The delithiation at initial cycles is solely carried out by a conversion reaction of Li metal. When the overpotential of the anode increases over the delithiation potential of lithiated graphite after cycling, a deintercalation reaction is consequently triggered to complete a whole CTD delithiation process, largely reducing the formation of dead Li due to a highly reversible deintercalation reaction. Under practical conditions, the working batteries based on a CTD delithiation mechanism maintain 210 cycles with a capacity retention of 80% in comparison to 110 cycles of a bare Li anode. Moreover, a 1 Ah pouch cell with a CTD delithiation mechanism operates for 150 cycles. The work ingeniously restrains the generation of dead Li by manipulating the delithiation mechanisms of the anode and contributes to a fresh concept for the design of practical composite Li anodes.

INTRODUCTION

Formidable environmental challenges, such as the massive emission of greenhouse gases, appeal for the utilization of renewable but intermittent energy sources based on solar, wind, and so on.[1] Consequently, a high-energy-density, low-cost, and long-cycling secondary battery to store intermittent energy sources for subsequent stable utilization, represented by lithium (Li)-ion batteries (LIBs), is gaining global witnesses and ever-increasing attention.[2−5] However, the specific energy of LIBs is approaching the theoretical limit (<350 Wh kg^{-1}) owing to the intercalation battery chemistry.[6]

Graphite based on an intercalation mechanism is widely accepted as an anode material for practical LIBs because the specific intercalation/deintercalation working mechanism of graphite minimizes the loss of active Li sources during the repeated cycles and significantly improves the cycle life.[7,8] However, the inferior theoretical specific capacity of the graphite anode (372 mAh g^{-1}) largely limits its further applications in terms of increasing energy density.[9] Exploring advanced anode materials with a high specific capacity based on a new working mechanism to replace graphite in routine LIBs is a primary strategy for achieving a battery with a higher energy density.[10]

Among various anode materials, Li metal based on a conversion mechanism (Li = $Li^+ + e^-$) renders an ultrahigh theoretical specific capacity of 3860 mAh g^{-1} and low reduction potential (−3.040 V vs standard hydrogen electrode), which has been considered as an ideal anode material for batteries.[11−13] The Li metal anode achieves the reversible storage/release of Li ions through a conversion

Received: August 16, 2021

reaction. However, a nonuniform Li stripping is hardly circumvented.[14,15] Partially active Li inevitably loses electronic contact with conductive networks due to the nonuniform stripping process, forming electrically isolated Li debris (usually named dead Li). The dead Li cannot be utilized as active materials during subsequent cycles, reducing the utilization efficiency of Li metal and thus inducing a short lifespan of a working battery,[16] especially under practical conditions including limited Li (<10 mAh cm^{-2}) and a low negative/positive capacity (N/P) ratio (<3).[17−19] Therefore, restraining the generation of dead Li is essential for the practical applications of a Li metal anode. Presently, tremendous efforts have been devoted to regulating the behaviors of Li plating/stripping based on a conversion reaction, such as electrolyte design,[20−24] artificial protective layers,[25,26] and 3D hosts.[27−31] The intrinsic nonuniform stripping of active Li stemmed from only the conversion reaction inevitably leads to the formation and accumulation of dead Li. Consequently, a new working mechanism is imperative to overcome the drawbacks of a mere conversion mechanism for the high utilization of a Li metal anode.

The increasing overpotential of Li stripping based on a conversion reaction during cycles inspires an ingenious working mechanism. The accumulation of dead Li on bulk Li limits the transport of Li ions and increases the overpotential of Li stripping continuously. The increase of overpotential provides an opportunity to switch the delithiation mechanism by introducing another material to finish the whole delithiation process, constructing a composite anode. The introduced additional material should possess a similar delithiation potential and a highly reversible storage/release mechanism of Li ions in order to achieve the switching of the delithiation mechanism.[32−34] Graphite based on the intercalation mechanism has a similar delithiation potential (0.1 V, vs Li/Li^+) to Li metal and a much higher utilization efficiency (>99.96%) presently.[35,36] In addition, various types of graphite can be chosen with sufficient technology maturity.

In this contribution, a successive conversion−deintercalation (CTD) delithiation mechanism is demonstrated to construct a practical Li metal−graphite (Li/C) composite anode. The conversion mechanism of Li metal works at initial cycles because the delithiation overpotential just exceeds the stripping potential of Li metal (0 V, vs Li/Li^+) (Figure 1a). However, the delithiation overpotential overlapped on the anode gradually increases over the deintercalation potential of lithiated graphite with the accumulation of dead Li (Figure 1b). At this stage, Li ions simultaneously delithiate from lithiated graphite and Li metal. The delithiation mechanism is triggered from a single conversion mechanism to the CTD delithiation mechanism, and the CTD delithiation mechanism continuously works during subsequent cycles since graphite is rapidly replenished by Li ions. The highly reversible deintercalation mechanism of lithiated graphite affords no generation of dead Li and thus reduces the accumulation of dead Li. Under practical conditions, the full cell with the CTD delithiation mechanism maintains 210 cycles with a capacity retention of 80% in comparison to a bare Li anode of 110 cycles. Moreover, a 1 Ah pouch cell with a Li/C composite anode performs 150 cycles with a small polarization.

RESULTS AND DISCUSSION

The achievement of a successive CTD delithiation mechanism is based on two key prerequisites. First, the delithiation

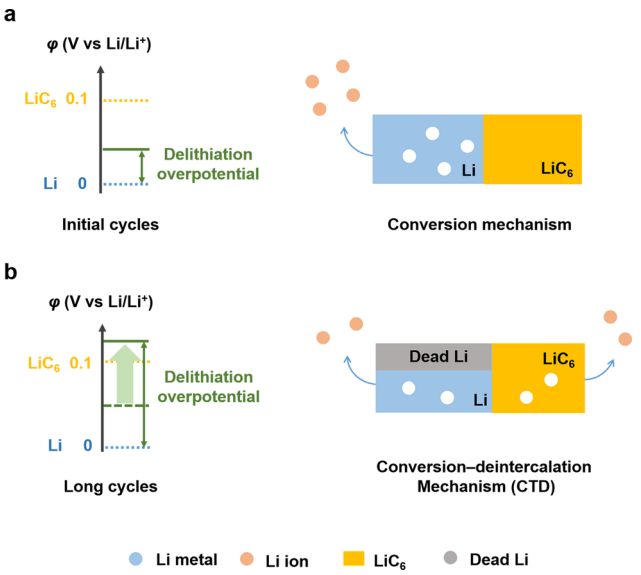

Figure 1. Schematic diagram of the delithiation mechanism of the composite anode (a) at initial cycles and (b) after long cycles.

overpotential accumulated on the anode during cycles should be larger than the deintercalation potential of lithiated graphite, which is generally considered to be 0.1 V (vs Li/Li^+).[37,38] Second, the intercalation rate of Li ions to graphite should be no less than the delithiation rate of Li ions from the whole anode to ensure the deintercalation mechanism continuously contributes to the capacity throughout the delithiation process. Accordingly, a Li/C composite anode with a bilayer structure was designed (Figures S1−S4).

A three-electrode test was implemented to accurately monitor the overpotential evolution of the Li/C composite anode during practical cycles (Figure S5). The three-electrode setup employs a Li@Cu as the reference electrode as reported.[39] The potential of the Li/C composite anode is less than 20 mV (vs Li/Li^+) at the third cycle and increases to 0.1 V (vs Li/Li^+) after 15 cycles (Figure 2a). In contrast, the potential evolution of graphite changes little during cycling, and the initial deintercalation potential is maintained at 0.1 V (vs Li/Li^+). The two potential profiles have an obvious crossover after the 15th cycle, which implies the possibility of Li ions deintercalating from lithiated graphite. The average overpotential of a composite anode is illustrated in Figure 2b. The overpotential of a Li/C composite anode is gradually elevated and exceeds the deintercalation potential of lithiated graphite at the 15th cycle. Therefore, the deintercalation mechanism is triggered to compensate for a single conversion mechanism, achieving the successive CTD delithiation mechanism as illustrated in Figure 1b. In addition, the ratio of overpotential on the anode over 0.1 V (vs Li/Li^+) at each cycle approaches 100% after 15 cycles (Figure 2c), and thus the CTD delithiation mechanism can dominate during the continuous delithiation process.

In order to directly confirm that Li ions in lithiated graphite can deintercalate during repeated cycles, the cycled electrode was investigated by X-ray diffraction (XRD) and time-of-flight secondary ion mass spectrometry (TOF-SIMS).[40] A specific circular electrode comprising a semicircular Li metal and a semicircular graphite electrode was designed as a working electrode. With this specific structure, the diffusion of Li ions from Li metal to graphite was significantly blocked due to the

https://doi.org/10.1021/jacs.1c08606
J. Am. Chem. Soc. XXXX, XXX, XXX−XXX

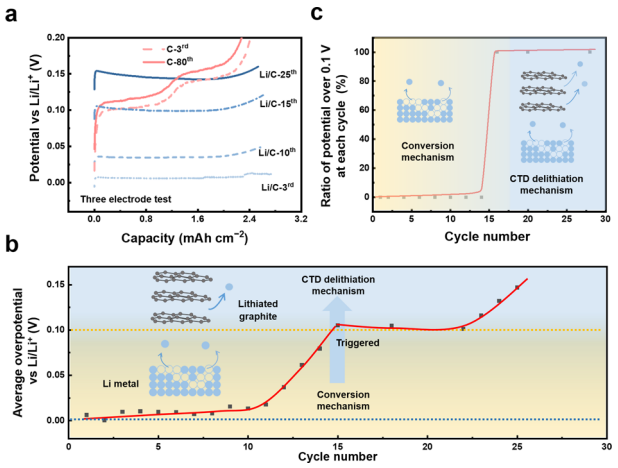

Figure 2. (a) Delithiation potential of the composite anode measured by a three-electrode test. (b) Profile of average overpotential with the cycle number in the three-electrode test. The average overpotential is defined as the arithmetic mean of the overpotential at different delithiation capacities each cycle. (c) Relationship between the ratio of potential over 0.1 V and the cycle number in the three-electrode test.

limited contact area compared with the vertical bilayer structure (Figure 3a).

Bare Li was employed as a counter electrode, and the testing cell was cycled at a current density of 1.0 mA cm^{-2} and an areal capacity of 3.0 mAh cm^{-2}. The graphite anode is intercalated by Li ions to form LiC_6 in the first plating process, and the voltage during the process of delithiation is less than 0.1 V at the second cycle since Li ions are preferentially stripped from the semicircular Li metal due to the low potential (Figure 3a,b). The sole signal of LiC_6 demonstrates that Li ions in LiC_6 cannot be employed during the initial cycles (Figure 3c). When the dead Li accumulates on the surface of Li metal after cycling, the voltage is elevated over 0.1 V. The signal of LiC_{12} emerges at the 15th cycle, and the ratio of peak area of LiC_6 and LiC_{12} reduces to 0.58:1 from 0.83:1 during the process of delithiation, confirming that Li ions can deintercalate from the semicircular lithiated graphite anode. The distribution of Li ions in the bulk semicircular graphite electrode after 15 cycles was investigated by TOF-SIMS (Figure S6). The position of graphite, such as part 1 and 2, is confirmed by the mapping of C^- (Figure 3d). The intensities of Li ions in part 1 and 2 have an obvious distinction, which demonstrates that Li ions in part 2 have deintercalated during the delithiation process, and the results agree well with the XRD analysis (Figure 3e).[41] In addition, when Li ions deintercalate from lithiated graphite, partial deposited Li metal remains on the surface of graphite according to the mapping of Li_2^-. This result further elucidates that the delithiation mechanism is composed of the deintercalation and conversion mechanism rather than being simply determined by the conversion mechanism (Figure 3f).

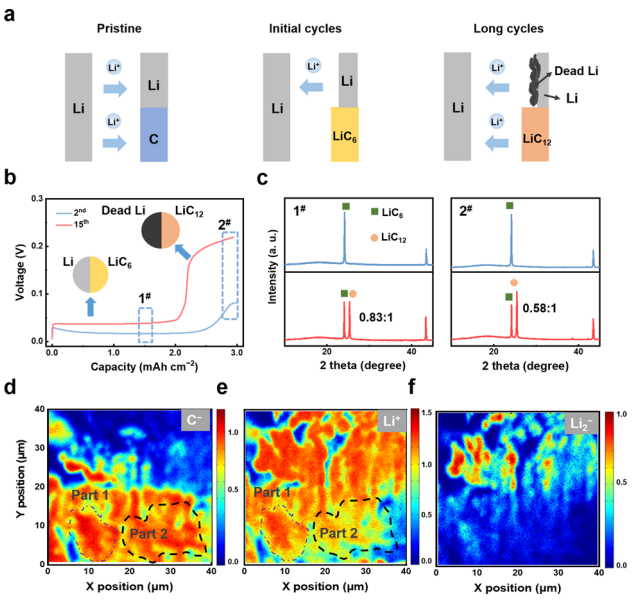

Figure 3. (a) Schematic diagram of the working state of a specific cell at the pristine state (left panel), initial cycles (middle panel), and after long cycles (right panel). (b) Voltage−capacity curves of the above cell at the 2nd and 15th cycle. (c) XRD patterns of the semicircular graphite electrode in Figure 3b. The blue and red lines represent the 2nd and 15th cycle, respectively. 1# and 2# represent the middle and terminal state of charge, respectively. (d) C^-, (e) Li^+, and (f) Li_2^- mapping of the semicircular graphite electrode in Figure 3b after 15 cycles by TOF-SIMS after depth sputtering.

Li ions in graphite should be quickly replenished from bulk Li metal after deintercalation in order to achieve the CTD delithiation mechanism working throughout the delithiation process. The intercalation of Li ions to graphite to form LiC_6 during the delithiation process results from two patterns: solid diffusion and an electrochemical process (Figure 4a). One pattern is the solid diffusion from the direct contact between Li metal and graphite. The solid diffusion coefficient is estimated to be 0.2×10^{-8} cm^2 s^{-1}, which is sluggish at room temperature and cannot replenish Li ions as soon as possible.[42] Accordingly, the signal of bare graphite remains strong when

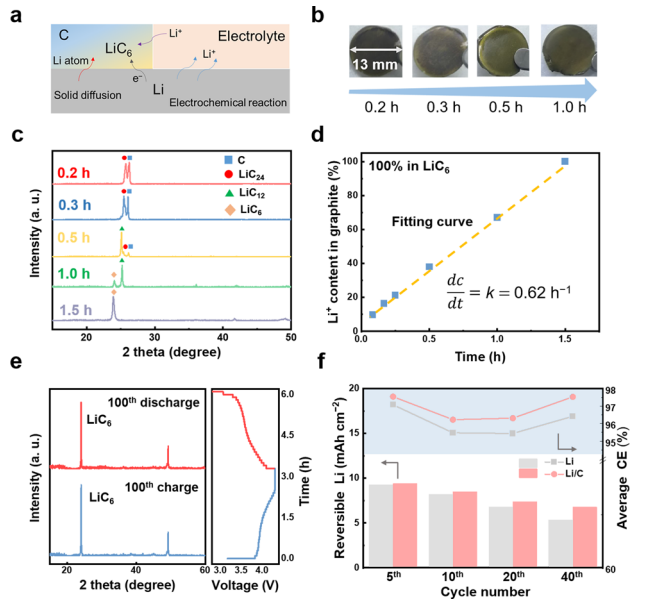

Figure 4. (a) Schematic diagram of the formation mechanism of LiC_6. (b) Color and (c) XRD patterns of the graphite electrode under different rest durations. (d) Calculation of kinetic parameters for the formation of LiC_6 in the Li/C composite anode. (e) XRD patterns of the composite anode at the 100th cycle in a full cell and the corresponding voltage profiles. (f) Average CE and reversible Li at different cycles with bare Li and a Li/C composite anode.

https://doi.org/10.1021/jacs.1c08606
J. Am. Chem. Soc. XXXX, XXX, XXX−XXX

the graphite electrode is pressed on a Li foil in a coin cell without electrolyte after 3.0 h (Figures S7 and S8).

The other pattern is the intercalation of Li ions induced by an electrochemical process. A primary cell forms due to the discrepancy of the thermodynamic potential between graphite and Li metal. Li ions in the electrolyte intercalate in graphite, and the electron transfer relies on the solid−solid connection between graphite and Li metal. An obvious color change can be observed from the disassembled cells in the presence of electrolyte, and the gold color of LiC_6 can be visualized after 1.0 h (Figure 4b).[43] The kinetics of the re-formation of LiC_6 was investigated by XRD under different shelving durations in coin cells.[44] From the XRD patterns, only the signature of graphite can be observed in the pristine Li/C composite anode. The peak of LiC_{24} appears after 0.2 h, and LiC_{12} becomes the main component after 0.5 h. The peak of graphite disappears after 1.0 h. There is only a LiC_6 peak in the XRD pattern of the graphite electrode after 1.5 h (Figure 4c). The concentration of Li ion in lithiated graphite was calculated according to the area of the peak in the XRD patterns, assuming the concentration of Li ions in LiC_6 is 100% (Figure 4d). It is found that the concentration of Li ions in lithiated graphite has a linear relationship with the shelving time. Therefore, the Li-ion intercalating reaction in graphite can be fitted with the first-order reaction. The apparent kinetic parameter k is equated to 0.62 h^{-1}, indicating that graphite can be fully intercalated by Li ions to form LiC_6 within 1.6 h. In general, the rate of Li-ion stripping is determined by the cycle rate, which is set to 0.4 C (h^{-1}) in this work. The results confirm that the intercalation rate of Li ions to graphite is larger than the delithiation rate of Li ions from the whole anode. This conclusion was verified in a full cell pairing with a Li/C composite anode and $LiNi_{0.5}Co_{0.2}Mn_{0.3}O_2$ (NCM523) cathode. There is a LiC_6 peak during the process of charge and discharge at 0.4 C after 100 cycles, which demonstrates that the Li ions in graphite are quickly replenished to re-form LiC_6 after the deintercalation from lithiated graphite (Figure 4e).

At this stage, the two key prerequisites to achieve a successive CTD delithiation mechanism are solidly confirmed. The overpotential of Li stripping gradually increases during cycles and can exceed the deintercalation potential of lithiated graphite. Thus, the deintercalation mechanism will be triggered to implement the whole delithiation process in addition to the conversion mechanism, constructing a CTD delithiation mechanism. The quick intercalation of Li ions to graphite from bulk Li metal based on an electrochemical process ensures the continued working of the CTD delithiation mechanism. It is worth noting that the time when a CTD delithiation mechanism is triggered is impacted by the structure of the Li/C composite anode and cycle conditions, such as current density.

Benefiting from the deintercalation mechanism of lithiated graphite, which affords no generation of dead Li, the accumulation of dead Li on the Li/C composite anode is significantly reduced. The average Coulombic efficiency (CE) of the half-cell with bare Li is 97.1%, which is similar to 97.5% of the cell with a Li/C composite anode in the initial 5 cycles (Figure 4f). The difference of the irreversible Li is 0.12 mAh cm^{-2}, indicating that the utilization efficiency of Li ions is similar in the cell with different anodes and confirming that the delithiation mechanisms are consistent at initial cycles. However, the gap between the average CE and reversible Li is gradually enlarged between the different anodes during cycling. The average CE of bare Li is 95.4% and 96.4% after 20 and 40 cycles, respectively, which is less than 96.3% and 97.5% of a Li/C composite anode. Meanwhile, the reversible Li capacity is 6.78 mAh cm^{-2} in a Li/C composite anode, which is higher than that in a bare Li anode of 5.53 mAh cm^{-2} after 40 cycles (Figures 4f and S9). The difference in reversible capacity between the two anodes after 40 cycles is 10 times larger than that after the fifth cycle. The improved average CE and reversible Li stem from the involvement of the deintercalation mechanism from lithiated graphite. The deintercalation reaction in the CTD delithiation mechanism effectively circumvents the generation of dead Li induced by only a conversion reaction.

In addition, the volume expansion after repeated cycles is ameliorated, which can be attributed to the decrease of dead Li with the CTD delithiation mechanism. Scanning electron microscopy (SEM) images reveal that a bare Li anode exhibits a huge volume expansion of 58% after 40 cycles at 1.0 mA cm^{-2} and 3.0 mAh cm^{-2}. In contrast, the volume expansion is only 14% for a Li/C composite anode under the same conditions (Figure S10). There is considerable dead Li on the surface of a bare Li anode, but less dead Li is observed on a Li/C composite anode due to the decreased capacity via a conversion mechanism (Figure S11). The bare Li | Li symmetric cell exhibits a gradually increasing polarization to 500 mV within 200 h, while the Li/C | Li/C symmetric cell maintains a much lower and more stable polarization of 250 mV after 350 h (Figure S12). The polarization voltage of a bare Li anode after cycling sharply increases compared with that of a Li/C composite electrode owing to the large volume expansion and thick dead Li layer. The restrained volume expansion and reduced polarization voltage of the Li/C composite electrode demonstrate the positive effect of the CTD delithiation mechanism in achieving superior electrochemical performance.

The full coin cells are assembled to probe the practical potential of the Li/C composite anode with the CTD delithiation mechanism. The capacity retention of the Li/C | NCM523 battery maintains 80% for 210 cycles at 0.4 C compared with 110 cycles of that with a bare Li anode (Figure 5a). Compared with a huge polarization voltage of 450 mV in a full cell with a bare Li anode at the 110th cycle, the full cell with a Li/C composite anode experiences a much smaller polarization voltage of 340 mV according to dV/dQ analysis, which is attributed to the reduced accumulation of dead Li (Figures 5b and S13). Benefiting from the reduced accumulation of dead Li, the fading tendency of capacity significantly decreases in full cells. The decline rate of capacity between adjacent cycles reaches 2.0% at the 100th cycle for a bare Li anode but maintains 1.0% over 200 cycles for a Li/C composite anode, which demonstrates the reduced consumption of active Li metal based on the CTD delithiation mechanism (Figure S14). The cycle performance of cells improves with the increased thickness of graphite on Li metal (Figure S15). Moreover, the Li/C composite anode was further employed in pouch cells matching with a high areal loading NCM523 cathode of 4.0 mAh cm^{-2}. The 1 Ah pouch cell performs 150 cycles at 0.1 C with a small polarization, indicating the practical potential of the CTD delithiation mechanism (Figure 5c and d). The specific capacity of the composite anode in this work is 1500 mAh g^{-1} (Figure S16). The specific capacity of the composite anode can be adjusted by changing the mass fraction of Li metal (Figure 5e). The

https://doi.org/10.1021/jacs.1c08606
J. Am. Chem. Soc. XXXX, XXX, XXX−XXX

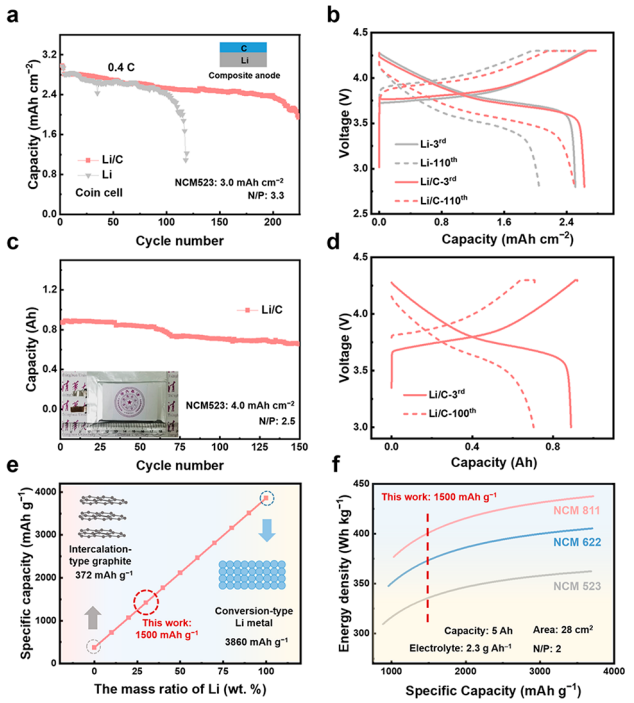

Figure 5. Cycling performance of coin and pouch cells. (a) Cycling performance of coin cells with different anodes and NCM523 cathode at 0.4 C. The localized high concentration electrolyte (LHCE) consists of LiFSI, DMC, and HFE with a mole ratio of 1.0:1.8:2.0, which was employed as the electrolyte. (b) Corresponding voltage profiles of coin cells at the 3rd and 110th cycle with bare Li and a Li/C composite anode. (c) Cycling performance of a 1 Ah pouch cell with a Li/C anode and NCM523 cathode at 0.1 C and the digital image of the pouch cell as an inset. The electrolyte was 1.0 M $LiPF_6$ dissolved in FEC/DMC (1:4, by volume). (d) Voltage−capacity profiles of a pouch cell at the 3rd and 100th cycle. (e) Relationship between the specific capacity of a composite anode and the mass ratio of Li metal. (f) Relationship between the specific energy based on the whole mass of the battery and the specific capacity of a composite anode pairing with different typical cathodes.

specific energy of the pouch cell is calculated based on the parameters in previous work.[45,46] With the Li/C composite anode and $LiNi_{0.8}Co_{0.1}Mn_{0.1}O_2$ (NCM811) cathode, the specific energy of the pouch cell can approach 400 Wh kg^{-1} (Figure 5f). In addition to the bare Li metal anode, the Li/C composite anode with a CTD delithiation mechanism provides a promising strategy to construct a practical high-energy-density Li metal battery with a long lifespan.

CONCLUSION

In conclusion, a successive conversion−deintercalation delithiation mechanism was demonstrated to construct a practical Li metal−graphite composite anode. A conversion mechanism of Li metal works due to the overpotential of less than 0.1 V (vs Li/Li$^+$) in the initial cycles. A deintercalation reaction of lithiated graphite will be consequently involved to complete a whole delithiation process when the overpotential of the anode exceeds the deintercalation potential of lithiated graphite due to the accumulation of dead Li. The deintercalation mechanism can continuously contribute to the capacity during the delithiation process since Li ions are rapidly replenished to graphite. No obvious dead Li is generated through a deintercalation mechanism, and thus the accumulation of dead Li is reduced during subsequent cycles. The full cell with a Li/C composite anode based on the CTD delithiation mechanism maintains 210 cycles with a capacity retention of 80% in comparison to a bare Li anode of 110 cycles under practical conditions. Moreover, a 1 Ah pouch cell performs 150 cycles, confirming the practical application potential of the CTD delithiation mechanism. This work demonstrates a fresh delithiation mechanism based on the deep insight into the overpotential evolution of a Li metal anode and affords a promising design of practical composite anodes for long-cycling high-energy-density rechargeable batteries.

ASSOCIATED CONTENT

Supporting Information

The Supporting Information is available free of charge at https://pubs.acs.org/doi/10.1021/jacs.1c08606.

Discussions of experimental details, figures of SEM and XRD, the morphology of bare Li and Li/C composite anode, the voltage profile of symmetric cells, and typical Li stripping curves of Li/C composite anodes (PDF)

AUTHOR INFORMATION

Corresponding Authors

Qiang Zhang − *Beijing Key Laboratory of Green Chemical Reaction Engineering and Technology, Department of Chemical Engineering, Tsinghua University, Beijing 100084, China;* orcid.org/0000-0002-3929-1541; Email: zhangqiang@mails.tsinghua.edu.cn

Xue-Qiang Zhang − *Advanced Research Institute of Multidisciplinary Science, Beijing Institute of Technology, Beijing 100081, China; School of Materials Science and Engineering, Beijing Institute of Technology, Beijing 100081, China;* orcid.org/0000-0003-2856-1881; Email: zhangxq@bit.edu.cn

Authors

Peng Shi − *Beijing Key Laboratory of Green Chemical Reaction Engineering and Technology, Department of Chemical Engineering, Tsinghua University, Beijing 100084, China*

Li-Peng Hou − *Beijing Key Laboratory of Green Chemical Reaction Engineering and Technology, Department of Chemical Engineering, Tsinghua University, Beijing 100084, China*

Cheng-Bin Jin − *Beijing Key Laboratory of Green Chemical Reaction Engineering and Technology, Department of Chemical Engineering, Tsinghua University, Beijing 100084, China*

Ye Xiao − *Advanced Research Institute of Multidisciplinary Science, Beijing Institute of Technology, Beijing 100081, China; School of Materials Science and Engineering, Beijing Institute of Technology, Beijing 100081, China*

Yu-Xing Yao − *Beijing Key Laboratory of Green Chemical Reaction Engineering and Technology, Department of Chemical Engineering, Tsinghua University, Beijing 100084, China*

Jin Xie − *Beijing Key Laboratory of Green Chemical Reaction Engineering and Technology, Department of Chemical Engineering, Tsinghua University, Beijing 100084, China*

Bo-Quan Li − *Advanced Research Institute of Multidisciplinary Science, Beijing Institute of Technology, Beijing 100081, China; School of Materials Science and*

Engineering, Beijing Institute of Technology, Beijing 100081, China; orcid.org/0000-0002-9544-5795

Complete contact information is available at: https://pubs.acs.org/10.1021/jacs.1c08606

Author Contributions

The manuscript was written through contributions of all authors. All authors have given approval to the final version of the manuscript.

Notes

The authors declare no competing financial interest.

■ ACKNOWLEDGMENTS

This work was supported by Beijing Municipal Natural Science Foundation (Z20J00043), National Key Research and Development Program (2021YFB2500300), National Natural Science Foundation of China (21825501, 22109007, and 52103342), China Postdoctoral Science Foundation (BX2021136 and 2021M691712), the Shuimu Tsinghua Scholar Program, and Tsinghua University Initiative Scientific Research Program.

■ REFERENCES

(1) Lin, D. C.; Liu, Y. Y.; Cui, Y. Reviving the Lithium Metal Anode for High-Energy Batteries. *Nat. Nanotechnol.* **2017**, *12* (3), 194−206.

(2) Cheng, X. B.; Zhang, R.; Zhao, C. Z.; Zhang, Q. Toward Safe Lithium Metal Anode in Rechargeable Batteries: A Review. *Chem. Rev.* **2017**, *117* (15), 10403−10473.

(3) Yoshino, A. The Birth of the Lithium-Ion Battery. *Angew. Chem., Int. Ed.* **2012**, *51* (24), 5798−800.

(4) Jin, C.; Sheng, O.; Chen, M.; Ju, Z.; Lu, G.; Liu, T.; Nai, J.; Liu, Y.; Wang, Y.; Tao, X. Armed Lithium Metal Anodes with Functional Skeletons. *Mater. Today Nano* **2021**, *13*, 100103.

(5) Cheng, X. B.; Liu, H.; Yuan, H.; Peng, H. J.; Tang, C.; Huang, J. Q.; Zhang, Q. A Perspective on Sustainable Energy Materials for Lithium Batteries. *SusMat* **2021**, *1* (1), 38−50.

(6) Lu, Y.; Rong, X.; Hu, Y.-S.; Chen, L.; Li, H. Research and Development of Advanced Battery Materials in China. *Energy Storage Mater.* **2019**, *23*, 144−153.

(7) Xu, K. Nonaqueous Liquid Electrolytes for Lithium-based Rechargeable Batteries. *Chem. Rev.* **2004**, *104* (10), 4303−417.

(8) Cai, W.; Yao, Y. X.; Zhu, G. L.; Yan, C.; Jiang, L. L.; He, C.; Huang, J. Q.; Zhang, Q. A Review on Energy Chemistry of Fast-Charging Anodes. *Chem. Soc. Rev.* **2020**, *49* (12), 3806−3833.

(9) Etacheri, V.; Marom, R.; Elazari, R.; Salitra, G.; Aurbach, D. Challenges in the Development of Advanced Li-Ion Batteries: A Review. *Energy Environ. Sci.* **2011**, *4* (9), 3243−3262.

(10) Chen, L.; Fan, X.; Ji, X.; Chen, J.; Hou, S.; Wang, C. High-Energy Li Metal Battery with Lithiated Host. *Joule* **2019**, *3* (3), 732−744.

(11) Zhang, X.-Q.; Zhao, C.-Z.; Huang, J.-Q.; Zhang, Q. Recent Advances in Energy Chemical Engineering of Next-Generation Lithium Batteries. *Engineering* **2018**, *4* (6), 831−847.

(12) Manthiram, A.; Fu, Y.; Chung, S. H.; Zu, C.; Su, Y. S. Rechargeable Lithium-Sulfur Batteries. *Chem. Rev.* **2014**, *114* (23), 11751−87.

(13) Bruce, P. G.; Freunberger, S. A.; Hardwick, L. J.; Tarascon, J. M. Li-O_2 and Li-S Batteries with High Energy Storage. *Nat. Mater.* **2012**, *11* (1), 19−29.

(14) Louli, A. J.; Li, J.; Trussler, S.; Fell, C. R.; Dahn, J. R. Volume, Pressure and Thickness Evolution of Li-Ion Pouch Cells with Silicon-Composite Negative Electrodes. *J. Electrochem. Soc.* **2017**, *164* (12), A2689−A2696.

(15) Gunnarsdottir, A. B.; Amanchukwu, C. V.; Menkin, S.; Grey, C. P. Noninvasive In Situ NMR Study of "Dead Lithium" Formation and Lithium Corrosion in Full-Cell Lithium Metal Batteries. *J. Am. Chem. Soc.* **2020**, *142* (49), 20814−20827.

(16) Han, Y.; Liu, B.; Xiao, Z.; Zhang, W.; Wang, X.; Pan, G.; Xia, Y.; Xia, X.; Tu, J. Interface Issues of Lithium Metal Anode for High-Energy Batteries: Challenges, Strategies, and Perspectives. *InfoMat* **2021**, *3* (2), 155−174.

(17) Shi, P.; Zhang, X. Q.; Shen, X.; Zhang, R.; Liu, H.; Zhang, Q. A Review of Composite Lithium Metal Anode for Practical Applications. *Adv. Mater. Technol.* **2020**, *5* (1), 1900806.

(18) Jin, C.; Liu, T.; Sheng, O.; Li, M.; Liu, T.; Yuan, Y.; Nai, J.; Ju, Z.; Zhang, W.; Liu, Y.; Wang, Y.; Lin, Z.; Lu, J.; Tao, X. Rejuvenating Dead Lithium Supply in Lithium Metal Anodes by Iodine Redox. *Nat. Energy* **2021**, *6* (4), 378−387.

(19) Liu, J.; Bao, Z. N.; Cui, Y.; Dufek, E. J.; Goodenough, J. B.; Khalifah, P.; Li, Q. Y.; Liaw, B. Y.; Liu, P.; Manthiram, A.; Meng, Y. S.; Subramanian, V. R.; Toney, M. F.; Viswanathan, V. V.; Whittingham, M. S.; Xiao, J.; Xu, W.; Yang, J. H.; Yang, X. Q.; Zhang, J. G. Pathways for Practical High-Energy Long-Cycling Lithium Metal Batteries. *Nat. Energy* **2019**, *4* (3), 180−186.

(20) Zhang, X. Q.; Chen, X.; Hou, L. P.; Li, B. Q.; Cheng, X. B.; Huang, J. Q.; Zhang, Q. Regulating Anions in the Solvation Sheath of Lithium Ions for Stable Lithium Metal Batteries. *ACS Energy Lett.* **2019**, *4* (2), 411−416.

(21) Sheng, O.; Zheng, J.; Ju, Z.; Jin, C.; Wang, Y.; Chen, M.; Nai, J.; Liu, T.; Zhang, W.; Liu, Y.; Tao, X. In Situ Construction of a LiF-Enriched Interface for Stable All-Solid-State Batteries and its Origin Revealed by Cryo-TEM. *Adv. Mater.* **2020**, *32*, 2000223.

(22) Wang, X. M.; Zhang, X. Q.; Shi, P.; Hou, L. P.; Zhou, M. Y.; Chen, A. B.; Zhang, Q. Glycolide Additives Enrich Organic Components in the Solid Electrolyte Interphase Enabling Stable Ultrathin Lithium Metal Anodes. *Mater. Chem. Front.* **2021**, *5* (6), 2791−2797.

(23) Wang, H.; Kim, S. C.; Rojas, T.; Zhu, Y.; Li, Y.; Ma, L.; Xu, K.; Ngo, A. T.; Cui, Y. Correlating Li-Ion Solvation Structures and Electrode Potential Temperature Coefficients. *J. Am. Chem. Soc.* **2021**, *143* (5), 2264−2271.

(24) Amanchukwu, C. V.; Yu, Z.; Kong, X.; Qin, J.; Cui, Y.; Bao, Z. A New Class of Ionically Conducting Fluorinated Ether Electrolytes with High Electrochemical Stability. *J. Am. Chem. Soc.* **2020**, *142* (16), 7393−7403.

(25) Wu, M.; Li, Y.; Liu, X.; Yang, S.; Ma, J.; Dou, S. Perspective on Solid-Electrolyte Interphase Regulation for Lithium Metal Batteries. *SmartMat* **2021**, *2* (1), 5−11.

(26) Duan, H.; Yin, Y. X.; Shi, Y.; Wang, P. F.; Zhang, X. D.; Yang, C. P.; Shi, J. L.; Wen, R.; Guo, Y. G.; Wan, L. J. Dendrite-Free Li-Metal Battery Enabled by a Thin Asymmetric Solid Electrolyte with Engineered Layers. *J. Am. Chem. Soc.* **2018**, *140* (1), 82−85.

(27) Shi, P.; Zhang, X. Q.; Shen, X.; Li, B. Q.; Zhang, R.; Hou, L. P.; Zhang, Q. A Pressure Self-Adaptable Route for Uniform Lithium Plating and Stripping in Composite Anode. *Adv. Funct. Mater.* **2021**, *31* (5), 2004189.

(28) Niu, C.; Pan, H.; Xu, W.; Xiao, J.; Zhang, J. G.; Luo, L.; Wang, C.; Mei, D.; Meng, J.; Wang, X.; Liu, Z.; Mai, L.; Liu, J. Self-Smoothing Anode for Achieving High-Energy Lithium Metal Batteries under Realistic Conditions. *Nat. Nanotechnol.* **2019**, *14* (6), 594−601.

(29) Jin, S.; Jiang, Y.; Ji, H.; Yu, Y. Advanced 3D Current Collectors for Lithium-Based Batteries. *Adv. Mater.* **2018**, *30* (48), 1802014.

(30) Chen, X.; Zhang, Q. Atomic Insights into the Fundamental Interactions in Lithium Battery Electrolytes. *Acc. Chem. Res.* **2020**, *53* (9), 1992−2002.

(31) Wang, L.; Zhou, Z.; Yan, X.; Hou, F.; Wen, L.; Luo, W.; Liang, J.; Dou, S. X. Engineering of Lithium-Metal Anodes towards a Safe and Stable Battery. *Energy Storage Mater.* **2018**, *14*, 22−48.

(32) Chu, Y.; Xi, B.; Xiong, S. One-Step Construction of MoO_2 Uniform Nanoparticles on Graphene with Enhanced Lithium Storage. *Chin. Chem. Lett.* **2021**, *32* (6), 1983−1987.

(33) Li, Y.; Du, Y. F.; Sun, G. H.; Cheng, J. Y.; Song, G.; Song, M. X.; Su, F. Y.; Yang, F.; Xie, L. J.; Chen, C. M. Self-Standing Hard Carbon Anode Derived from Hyper-Linked Nanocellulose with High

Cycling Stability for Lithium-Ion Batteries. *EcoMat* **2021**, *3* (2), 12091.
(34) Wang, K.; Xu, Y.; Wu, H.; Yuan, R.; Zong, M.; Li, Y.; Dravid, V.; Ai, W.; Wu, J. A Hybrid Lithium Storage Mechanism of Hard Carbon Enhances its Performance as Anodes for Lithium-Ion Batteries. *Carbon* **2021**, *178*, 443−450.
(35) Chen, K. H.; Namkoong, M. J.; Goel, V.; Yang, C. L.; Kazemiabnavi, S.; Mortuza, S. M.; Kazyak, E.; Mazumder, J.; Thornton, K.; Sakamoto, J.; Dasgupta, N. P. Efficient Fast-Charging of Lithium-Ion Batteries Enabled by Laser-Patterned Three-Dimensional Graphite Anode Architectures. *J. Power Sources* **2020**, *471*, 228475.
(36) Burns, J. C.; Stevens, D. A.; Dahn, J. R. In-Situ Detection of Lithium Plating Using High Precision Coulometry. *J. Electrochem. Soc.* **2015**, *162* (6), A959−A964.
(37) Son, Y.; Lee, T.; Wen, B.; Ma, J.; Jo, C.; Cho, Y.-G.; Boies, A.; Cho, J.; De Volder, M. High Energy Density Anodes Using Hybrid Li Intercalation and Plating Mechanisms on Natural Graphite. *Energy Environ. Sci.* **2020**, *13* (10), 3723−3731.
(38) Li, Y.; Lu, Y.; Adelhelm, P.; Titirici, M. M.; Hu, Y. S. Intercalation Chemistry of Graphite: Alkali Metal Ions and Beyond. *Chem. Soc. Rev.* **2019**, *48* (17), 4655−4687.
(39) Yao, Y. X.; Chen, X.; Yan, C.; Zhang, X. Q.; Cai, W. L.; Huang, J. Q.; Zhang, Q. Regulating Interfacial Chemistry in Lithium-Ion Batteries by a Weakly Solvating Electrolyte. *Angew. Chem., Int. Ed.* **2021**, *60* (8), 4090−4097.
(40) Schweidler, S.; de Biasi, L.; Schiele, A.; Hartmann, P.; Brezesinski, T.; Janek, J. Volume Changes of Graphite Anodes Revisited: A Combined Operando X-ray Diffraction and In Situ Pressure Analysis Study. *J. Phys. Chem. C* **2018**, *122* (16), 8829−8835.
(41) Shi, P.; Li, T.; Zhang, R.; Shen, X.; Cheng, X. B.; Xu, R.; Huang, J. Q.; Chen, X. R.; Liu, H.; Zhang, Q. Lithiophilic LiC_6 Layers on Carbon Hosts Enabling Stable Li Metal Anode in Working Batteries. *Adv. Mater.* **2019**, *31* (8), 1807131.
(42) Gao, T.; Han, Y.; Fraggedakis, D.; Das, S.; Zhou, T. T.; Yeh, C. N.; Xu, S. M.; Chueh, W. C.; Li, J.; Bazant, M. Z. Interplay of Lithium Intercalation and Plating on a Single Graphite Particle. *Joule* **2021**, *5* (2), 393−414.
(43) Yang, W.; Xie, H.; Shi, B.; Song, H.; Qiu, W.; Zhang, Q. In-Situ Experimental Measurements of Lithium Concentration Distribution and Strain Field of Graphite Electrodes during Electrochemical Process. *J. Power Sources* **2019**, *423*, 174−182.
(44) Fujimoto, H.; Takagi, S.; Shimoda, K.; Kiuchi, H.; Okazaki, K.-I.; Murata, T.; Ogumi, Z.; Abe, T. Analysis of Intercalation/De-Intercalation of Li Ions Into/From Graphite at 0°C via Operando Synchrotron X-ray Diffraction. *J. Electrochem. Soc.* **2021**, *168* (9), 090515.
(45) Niu, C.; Lee, H.; Chen, S.; Li, Q.; Du, J.; Xu, W.; Zhang, J. G.; Whittingham, M. S.; Xiao, J.; Liu, J. High-Energy Lithium Metal Pouch Cells with Limited Anode Swelling and Long Stable Cycles. *Nat. Energy* **2019**, *4* (7), 551−559.
(46) Zhang, X. Q.; Li, T.; Li, B. Q.; Zhang, R.; Shi, P.; Yan, C.; Huang, J. Q.; Zhang, Q. A Sustainable Solid Electrolyte Interphase for High-Energy-Density Lithium Metal Batteries under Practical Conditions. *Angew. Chem., Int. Ed.* **2020**, *59* (8), 3252−3257.

https://doi.org/10.1021/jacs.1c08606
J. Am. Chem. Soc. XXXX, XXX, XXX−XXX